Albumin (BSA) adsorption onto graphite stepped surfaces

Pamela Rubio-Pereda, J. G. Vilhena, Noboru Takeuchi, Pedro A. Serena, and Rubén Pérez

Citation: The Journal of Chemical Physics **146**, 214704 (2017); doi: 10.1063/1.4984037
View online: http://dx.doi.org/10.1063/1.4984037
View Table of Contents: http://aip.scitation.org/toc/jcp/146/21
Published by the American Institute of Physics

Albumin (BSA) adsorption onto graphite stepped surfaces

Pamela Rubio-Pereda,[1,2,a)] J. G. Vilhena,[1,3,4,a)] Noboru Takeuchi,[5] Pedro A. Serena,[1] and Rubén Pérez[3,6,b)]

[1]*Instituto de Ciencia de Materiales de Madrid (ICMM), CSIC, c/ Sor Juana Inés de la Cruz 3, E-28049 Madrid, Spain*
[2]*Centro de Investigación Científica y de Educación Superior de Ensenada 3918, 22860 Ensenada, Baja California, Mexico*
[3]*Departamento de Física Teórica de la Materia Condensada, Universidad Autónoma de Madrid, E-28049 Madrid, Spain*
[4]*Department of Macromolecular Structures, Centro Nacional de Biotecnología, Consejo Superior de Investigaciones Científicas, 28049 Cantoblanco, Madrid, Spain*
[5]*Centro de Nanociencias y Nanotecnología, Universidad Nacional Autónoma de México, 22800 Ensenada, Baja California, Mexico*
[6]*Condensed Matter Physics Center (IFIMAC), Universidad Autónoma de Madrid, E-28049 Madrid, Spain*

(Received 28 January 2017; accepted 10 May 2017; published online 2 June 2017)

Nanomaterials are good candidates for the design of novel components with biomedical applications. For example, nano-patterned substrates may be used to immobilize protein molecules in order to integrate them in biosensing units. Here, we perform long MD simulations (up to 200 ns) using an explicit solvent and physiological ion concentrations to characterize the adsorption of bovine serum albumin (BSA) onto a nano-patterned graphite substrate. We have studied the effect of the orientation and step size on the protein adsorption and final conformation. Our results show that the protein is stable, with small changes in the protein secondary structure that are confined to the contact area and reveal the influence of nano-structuring on the spontaneous adsorption, protein-surface binding energies, and protein mobility. Although van der Waals (vdW) interactions play a dominant role, our simulations reveal the important role played by the hydrophobic lipid-binding sites of the BSA molecule in the adsorption process. The complex structure of these sites, that incorporate residues with different hydrophobic character, and their flexibility are crucial to understand the influence of the ion concentration and protein orientation in the different steps of the adsorption process. Our study provides useful information for the molecular engineering of components that require the immobilization of biomolecules and the preservation of their biological activity. *Published by AIP Publishing.* [http://dx.doi.org/10.1063/1.4984037]

I. INTRODUCTION

Biocompatible nanomaterials have attracted great attention in the bioengineering and biotechnology fields due to their use in the design of novel components with biomedical applications.[1–7] Some of these components require the immobilization of biomolecules onto substrates that preserve their biological activity. Although well-ordered nano-patterned surfaces already form part of bioassays and biosensors,[8,9] new artificially produced nano-patterned substrates are under intense investigation[4] since substrate properties can be tuned by patterning. Scanning probe microscopy (SPM) studies[4] have shown that step edges, where a higher chemical reactivity is expected, are indeed preferential sites for protein adsorption. Thus, an increase in the surface roughness provides more surface area for protein adsorption and anchorage. Furthermore, due to this enhanced interaction, surface nano-patterns with the same size or smaller than the adsorbates (e.g., in the range of 3–15 nm common to most blood proteins[10]) could induce a controlled change in the protein conformation.

Nano-patterned substrates made of carbon-based materials, such as graphene layers, are good candidates in the design of novel components for biomedical applications. The unique properties of graphene have already made it a promising material for many applications, including electronic devices, energy storage, and nanocomposites. The formation of well-ordered nano-patterned graphite substrates is now possible thanks to low-cost patterning methods.[8,9] Furthermore, the ability of graphene layers to be biofunctionalized has been tested in numerous biotechnological applications such as biomolecule-assisted exfoliation and dispersion of graphene and other two-dimensional materials,[11,12] building adaptable or multifunctional bioplatforms,[13] measuring biological entities, and electrical stimulation of cells.[14–18]

Computer simulations are nowadays an essential tool to explore very complex phenomena on material science and biosystems and to understand and extract quantitative information from experimental results.[19–22] In particular, protein/substrate interactions have been extensively explored with molecular dynamics (MD) simulations.[22–32] MD simulations provide insight into the atomistic mechanisms involved in the adsorption process. In the case of nano-patterning, they offer a way to discriminate among the properties emerging from the

[a)]P. Rubio-Pereda and J. G. Vilhena contributed equally to this work.
[b)]Electronic mail: ruben.perez@uam.es

substrate topography (size and shape) from those associated with the chemical composition.

MD simulations of the adsorption of biological molecules on stepped graphite substrates, which can be easily modeled by the stacking of few graphene layers, open the way to explore the influence of surface nano-patterns on protein adsorption and the resulting structural changes. This study is not only relevant for the fundamental understanding of the protein adsorption process but also has possible technological implications due to the growing use of graphene in biological and biomedical applications.[3,14,15,33–38]

Bovine serum albumin (BSA), one of the most abundant protein in blood serum,[39] is an ideal candidate for this MD study. Serum albumins have been used for many years as a model protein in biophysical, biochemical, and physicochemical studies.[40,41] The human serum albumin (HSA) acts as a molecular transport via nonspecific interactions for hydrophobic ligands such as fatty acids, steroids, anaesthetics, and other specific compounds present in the human blood plasma. Although the HSA is a more important protein in medical studies to understand the protein-surface affinity, BSA is widely used as a model protein in SPM experiments to study specifically molecular adsorption and mobility.[41–43] BSA is characterized by its low cost availability, possessing a structure, and binding properties very similar to the HSA. Furthermore, BSA is believed to be the first constituent to be adsorbed onto surfaces exposed to a biological media.[1] Given that platelets (which are able to trigger nonspecific immune responses such as inflammation and thrombosis which preclude the rejection of an implant) can adhere to adsorbed albumin only if albumin undergoes more than a 34% loss in its α-helical content,[7,44] it is of paramount importance to determine how a common feature present in graphite surfaces such as steps affects the degree of unfolding of this protein.

Here, we perform long MD simulations (up to 200 ns) using an explicit solvent and physiological ion concentrations to characterize the initial steps of BSA adsorption onto a nano-patterned graphite substrate. We have considered two different protein orientations and stepped graphite substrates with different number of graphene layers in order to study the effect of the orientation and step size on the protein adsorption and final conformation. This work is based on our previous study of the adsorption of BSA on a graphene bilayer,[45] where we showed, contrary to previous studies using implicit solvent methods,[22–28] that free adsorption takes place on two different orientations with minor structural rearrangements. A recent experimental work,[11] carried out by leading research groups from Manchester, was able to solve the contradictions in the reported biocompatibility of graphene-related systems. Their findings support our previous observations,[45] experimentally confirming that albumin retains its structure once it is adsorbed on graphene. Now, we explore how the adsorption on this hydrophobic surface is affected by the ion concentration and the substrate nano-structure, paying particular attention to the spontaneous character of the adsorption process. We follow the changes in the protein conformation, looking closely to the evolution of the protein secondary structure that plays a fundamental role in the BSA biological activity. We also explore the influence of nano-structuring on the protein-surface contact area and binding energies and the implications for protein mobility. Our results show that the protein is stable, with small changes in the protein secondary structure that are mostly located in the contact area. Although van der Waals (vdW) interactions play a dominant role, our simulations reveal the important role played by the hydrophobic lipid-binding sites of the BSA molecule in the adsorption process. The complex structure of these sites, that incorporate residues with different hydrophobic character, and their flexibility are crucial to understand the influence of the ion concentration and protein orientation in the different steps of the adsorption process. We believe that this extensive MD simulation study of protein adsorption on nano-patterned substrates under physiological conditions brings relevant information for the design of novel biomedical devices.

The rest of the paper is organized as follows: in Sec. II, we describe the computational method along with the simulation elements (substrate, protein, and solvent). Section. III presents the simulations for the different orientations and step sizes, including the binding energy, the contact area, the evolution of the protein secondary structure, and the distribution of residues around the protein-substrate contact area. Based on these results, we discuss the influence of ion concentration and nano-patterning on the adsorption process in Sec. IV. Finally, in Sec. V, we summarize the main messages of this study.

II. METHODS

A. Graphite substrates

Flat and stepped graphite substrates were considered to study their effect upon protein adsorption and conformation. An ordinary flat graphite substrate was compared with two stepped graphite substrates of specific heights. All substrates were constructed by the stacking of graphene layers in an A-B-A configuration.

The first substrate was a flat surface (labeled as "G0") made by stacking three equally sized graphene layers of 16×16 nm^2, as shown in Fig. 1(a). The G3 substrate [Fig. 1(b)] is a system consisting of two (16×16 nm^2) stacked graphene layers plus three smaller (8×16 nm^2) graphene layers on top. The G5 substrate [Fig. 1(c)] is a system consisting of two (16×16 nm^2) stacked graphene layers plus five smaller (8×16 nm^2) graphene layers on top. The G3 and G5 substrates have step heights of around 10.20 Å and 17.00 Å, respectively.

The presence of a rigid bulk substrate was modeled by restraining the motion of all atoms belonging to the bottom-most graphene layer.[45] In order to model graphene, we used the OPLS (Optimized Potentials for Liquid Simulations) aromatic carbon force field present on the AMBER (Assisted Model Building with Energy Refinement) generalized force field.[46] This force field is known to properly describe biological systems[47] and accurately reproduce graphene mechanical and hydration properties.[48] Furthermore recent joint experimental and theoretical work[20,49] showed that this force field is capable of not only correctly characterizing the adsorption process of a large protein (antibody) onto a graphene surface but also to properly describe the graphene tribological properties.

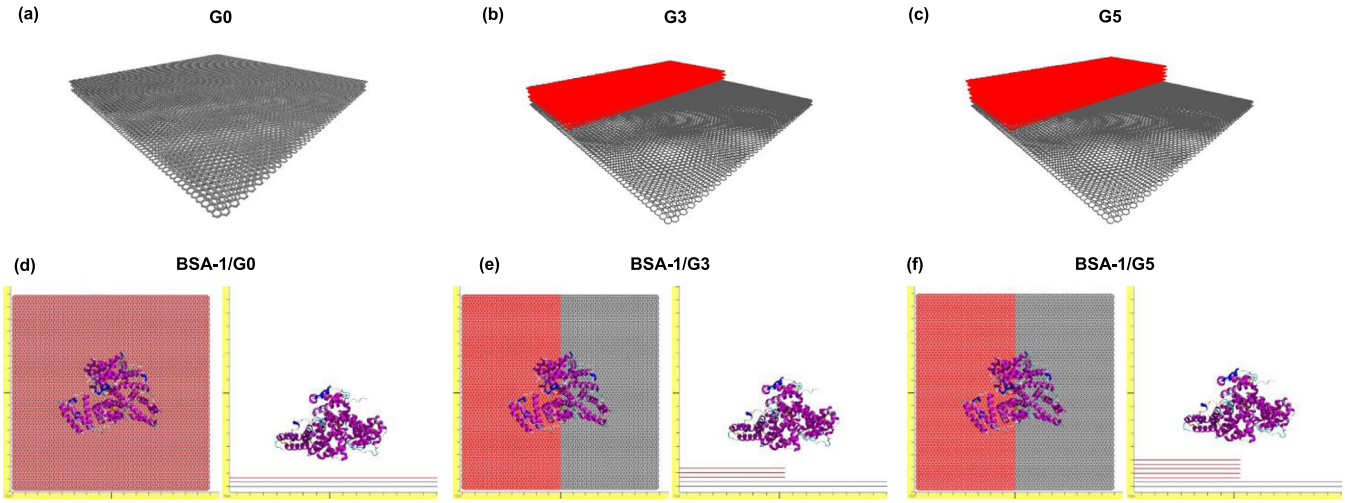

FIG. 1. [(a)–(c)] A schematic view of graphite substrates: (a) G0: a flat surface constructed by three stacked graphene layers; (b) G3: a surface with a three graphene layer step height; and (c) G5: a surface with a five graphene layer step height. [(d)–(f)] Top and side views of the graphite substrates with the BSA molecule in orientation 1 (BSA-1): (d) G0; (e) G3; and (f) G5. In each case, the BSA center of mass (x and y coordinates) is located exactly above the geometrical center of the lowest graphene layer. The initial distance between the uppermost graphene layer and the BSA atom closest to the surface is 10 Å.

At last, it is worthwhile mentioning that by modeling the substrates as above mentioned, one is able to mimic nano-patterned substrates. This follows from the fact that nowadays, the minimum separation distance between consecutive steps in nano-patterned substrates ranges 10-30 nm.[9,50,51] Since in our simulations the largest graphene layers had a size of 16×16 nm^2, it is safe to assume that the conclusions drawn from our work could be extended to nano-patterned surfaces with a periodicity equal or above 16 nm.

B. Biological molecule: Bovine serum albumin (BSA)

The BSA molecule has a molecular weight of approximately 67 kDa and its secondary structure is essentially constituted by α-helix (>73%). The X-ray crystallographic structure of BSA dimer was obtained from the protein data bank[52] with the PDB code 4f5s.[40] We then extracted the atomic coordinates of one BSA monomer and discarded the second BSA monomer as well as the polyethylene glycol (PEG) ligand. Protons were added to the protein structure according to the calculated ionization states[53] of its titratable groups at a pH of 7.4, resulting in a net-charge of 12 e. This selection of the pH value is in accordance with the blood pH[54] and with the pH of a FITC-BSA-M199-HEPES standard set used in BSA protein mobility experiments.[55] The AMBER ff99SB force field[56,57] was used in order to model the properties of the BSA molecule.

As all the other albumins, BSA is composed of three structurally similar domains, i.e., Domain 1 (D1), Domain 2 (D2), and Domain 3 (D3), each composed by two sub-domains, thus totaling six subdomains.[40,45] To make the analysis more clear, as in Refs. 58 and 59, here we consider that the BSA molecule is composed of two fragments, A and B, whose interface is held together by both hydrophobic and salt-bridge interactions.[59] In Fig. 2(a), we show the A and B fragments of BSA colored in gray and blue, respectively. The fragment B of the molecule contains a hydrophobic lipid-binding pocket, which is surrounded by α-helices identified in Fig. 2(a) by a red cylindrical-helix representation.

C. BSA/graphite systems

We simulate the BSA adsorption over graphite along two distinct orientations that have been considered in previous studies.[45,60] The choice of these two orientations[45] is motivated by the position of the Sudlow sites (DSs): the two main sites responsible for drug binding.[40] In the BSA-2 orientation, corresponding to the *O*2 orientation in Ref. 45 [see Fig. 2(b)], the DSs are far away from the surface, while in BSA-1 orientation [Fig. 2(c)], rotated by approximately 180° with respect to BSA-2 around an axis parallel to the graphene layers, these sites are close to it. The BSA-1 orientation not only allows us to bring the two sites as close as possible to the surface but it also exposes the bottom part of these pockets to the surface. Since these pockets are mostly composed of hydrophobic residues, this particular configuration might enhance the BSA adsorption process. The BSA-2 orientation positions the DSs away from the surface, thus attempting to mitigate the role played by these sites during the adsorption process.

It is important to stress that BSA-1 and BSA-2 orientations were chosen so as to understand how BSA key binding sites[40,45] affect and are affected by the adsorption to stepped surfaces. Although our simulations seem to indicate that the final adsorption configurations are stable, it could be that they are locked in meta-stable states. In order to determine what would be the most stable adsorption orientation, one should use instead advanced sampling methods such as parallel-tempering-Monte Carlo[61] or metadynamics[62] simulations. Alternatively, Zhou and co-workers have developed a method based on the concept of the hydrophobic dipole[63,64] that allows us to guess the most probable orientation by which a small protein may be adsorbed onto hydrophobic surfaces. This is an interesting idea and we have applied it to the two adsorption orientations considered in our study. Although this approach would suggest BSA-1 to be more stable than BSA-2 (in agreement with our results), still BSA-1 does not completely fulfill the rule that the hydrophobic dipole should be perpendicular to the substrate.[63,64] We suspect that this result

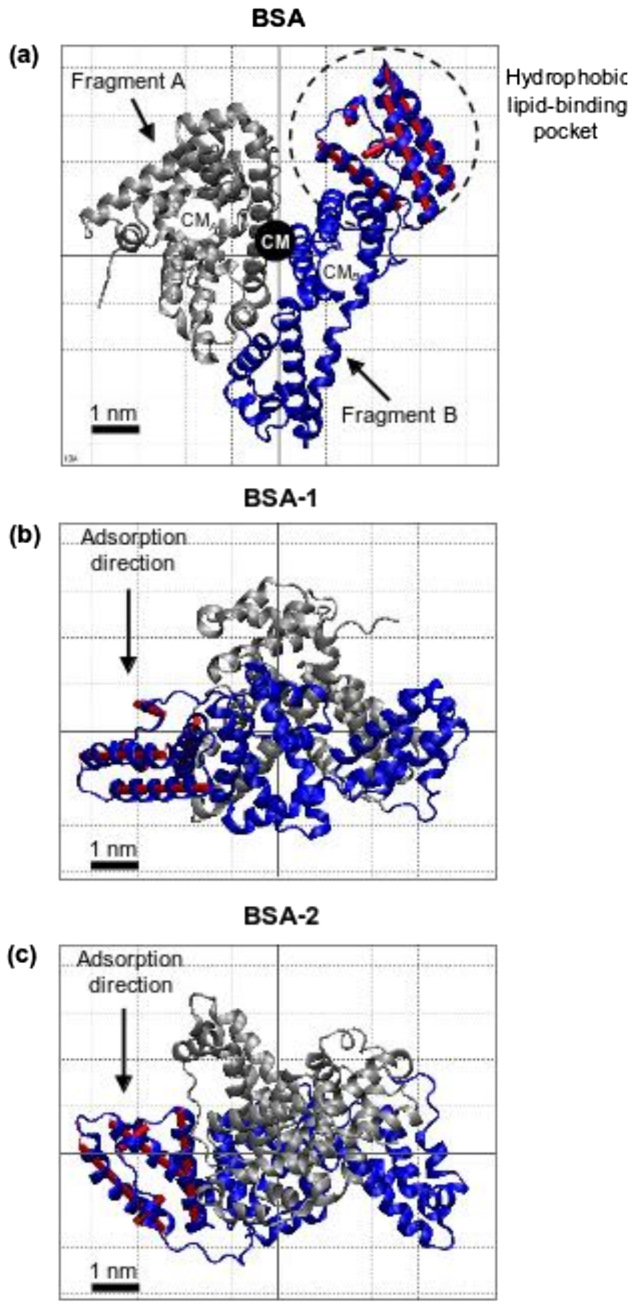

FIG. 2. (a) The structure of the BSA molecule, showing the A and B fragments of the BSA molecule (colored in gray and blue, respectively) and the center of mass positions for the A (CMA) and B (CMB) fragments and for the whole molecule (CM). The positions of the hydrophobic lipid-binding pocket, located in fragment B, and the surrounding α-helices are highlighted with red cylinders. (b) The BSA molecule in adsorption orientation 1 (labeled BSA-1). (c) BSA molecule in adsorption orientation 2 (labeled BSA-2). BSA-2 can be obtained by rotating approximately 180° the BSA-1 configuration around an axis parallel to the graphene layers.

is related to the size of BSA and more specifically to its complex structure that includes a combination of many large and small hydrophobic and hydrophilic patches.[40,45]

After the initial protein structure preparation, the BSA molecule was placed on top of each substrate in the two different orientations with its center of mass exactly above the geometrical center of the lowest graphene layer. The combination of the three substrates (G0, G3, and G5) with two orientations (BSA-1 and BSA-2) results in 6 different systems. Three of them, corresponding to the BSA-1 case, are shown in Figs. 1(d)–1(f). The initial distance between the uppermost graphene layer and the BSA atom closest to the surface is 10 Å. This distance guarantees a negligible protein-substrate interaction during the initial MD stages.

D. Solvation method

Despite the elevated computational cost, protein/substrate interactions are best described through the use of explicit solvent simulations.[45] Therefore each BSA/substrate system was solvated in a cubic box filled with water molecules represented by the TIP3P model.[65] This water model not only describes the interaction of water with proteins but also graphene's wetting properties.[22] We have used periodic boundary conditions with a cubic unit cell that extends 20 Å above the protein in the direction normal to the surface. The unit cell has been filled up with water molecules placed in such a way that the minimum solute–water distance is 1 Å. To account for proper physiological conditions, we have included salt ions in a concentration of 140 mM Na^+ and Cl^- (the total number of Na^+ and Cl^- ions ranges from 704 to 778, depending on the studied system), plus additional 12 Na^+ counter-ions for overall charge neutrality.

E. Molecular simulations

We used the AMBER12 software suite[56] with NVIDIA GPU (Graphics processing unit) acceleration.[57,66] Simulations were performed with periodic boundary conditions and particle mesh Ewald (with standard defaults and a real-space cutoff of 10 Å) was used to account for long-range electrostatic interactions. Van der Waals contacts were truncated at the real-space cutoff. The SHAKE algorithm was used to constrain bonds containing hydrogen, thus allowing us to use an integration step of 2 fs. Coordinates were saved every 1000 steps. A constant temperature of 300 K was ensured in all the simulations by means of a Langevin thermostat. For the MD simulations performed in the NTP ensemble, a Berendsen barostat was used to keep the pressure constant at 1 atm.

F. Protein adsorption protocol

Our simulation protocol is composed of 4 main stages: (1) energy minimization to prevent steric clashes arising from the system preparation; (2) thermalization process in which the temperature and pressure are kept constant at 300 K and 1 atm during 1 ns of simulation; (3) a 10 ns NVT simulation in which the protein (freely or forced, see below) is adsorbed over the surface; and (4) once BSA has reached (freely or forced) the surface, a ultra-long MD stage of up to 120 ns in a NVT ensemble is carried out for all the 6 protein-substrate configurations here considered.

In the third stage of the MD simulation protocol, we noticed that, in some cases, the protein-surface interaction was not strong enough to induce a spontaneous adsorption of BSA onto the substrate. For these configurations, we enhanced the diffusion/adsorption process by employing Steered MD (SMD) simulations to approach the protein until it gently touched the substrate. The SMD protocol consisted in moving

towards the surface a selected group of atoms at a constant velocity of 2.5 Å/ns via a harmonic restrain (with k = 50 kcal/mol). As the protein-substrate distance has in fact grown during the previous 10 ns of free MD, the SMD is applied during 4 ns in order to bring the protein and substrate into contact. This restrain is only applied to the alpha carbons belonging to 16 cysteine residues evenly distributed over the protein. The disulfide bonds formed between cysteine residues play an important role in the protein stability and, therefore, by selecting this group of atoms, we assured that no structural changes are induced due to the SMD simulation.

While for all the protein/surface configurations, we found that 120 ns of equilibration time sufficed to converge the structural parameters of the molecule [root-mean-square-distance (RMSD), the radius of gyration tensor (RGT), the contact surface area (CSA), and the total energy and its components]; for the G3 substrate, after this simulation time, some of these quantities were not fully converged. Therefore, for this particular case, we performed additional MD simulation thus totaling 200 ns of equilibration time.

G. Data analysis

In order to fully characterize the protein-surface adsorption process, we have used CPPTRAJ tools the AMBER package.[67] The evolution of the contact surface area (CSA) between the protein/substrate was calculated using the following definition:

$$CSA(t) = \frac{1}{2}\left(SASA_P(t) + SASA_S(t) - SASA_{P-S}(t)\right), \quad (1)$$

where the time dependent solvent-accessible-surface-area $SASA(t)$[68] was calculated for protein $[SASA_P(t)]$, substrate $[SASA_S(t)]$, and protein-substrate $[SASA_{P-S}(t)]$. In addition, the analysis of the changes of the BSA secondary structure upon adsorption was performed (for the different final adsorbed configurations) using the DSSP (Define Secondary Structure of Proteins) online software.[69,70]

In order to gather quantitative information about the influence of the substrate morphology on the BSA binding, we followed the evolution of the van der Waals (vdW) interaction of the protein, the substrate, and the combined system. As the graphene substrates are not charged, the only interactions between the protein and substrate will be entropic ones (hydrophilic forces) and vdW interactions. In our previous work,[45] we found for BSA adsorption to flat graphene that the adsorption free energy was dominated by the vdW interaction, with entropic effects contributing only 16% of the free energy difference between two different adsorption orientations.[45] Therefore we expect that the time evolution of the vdW interaction protein-surface, $E_{vdW}^{P-S}(t)$ will allow us to provide a rough estimate of the binding energies for each of the systems considered here. This quantity is determined using

$$E_{vdW}^{P-S}(t) = E_{vdW}^{total}(t) - E_{vdW}^{P}(t) - E_{vdW}^{S}(t), \quad (2)$$

where $E_{vdW}^{total}(t)$ stands for the vdW energy of the combined protein/substrate system, and $E_{vdW}^{P}(t)$ and $E_{vdW}^{S}(t)$ are the vdW energies of the isolated protein and substrate, respectively. These energies are computed from the protein and substrate structures extracted for each time step from our MD simulations and do not include the interaction with the water molecules. Although only the sum of all energy contributions is a true state function, $E_{vdW}^{P-S}(t)$ has been shown to be useful to understand the protein adsorption and desorption dynamics.[71]

III. RESULTS

A. BSA-1 and BSA-2 adsorption onto G0

We have first studied the adsorption process of BSA-1 and BSA-2 onto G0. Atomic structures after 1 ns of the thermalization process are shown in Figs. 3(a) and 3(b). During the first 10 ns of the molecular dynamics (MD) simulation, we observed that the BSA-1 molecule did not move towards the flat surface [Fig. 3(c)]. This behavior seems to indicate that the protein/substrate interaction is very weak at ionic concentrations (i.e., 140 mM of NaCl) that correspond to physiological conditions. Note that in the MD simulations for BSA and other proteins that we have performed so far,[20,45] we have always found a spontaneous and prompt adsorption to graphene. In order to enhance the adsorption process of the BSA-1/G0 system, we have used 4 ns SMD simulations in order to gently approach the protein to the substrate, as outlined in Sec. II. Figure S1 in the supplementary material shows the BSA-1 structures before and after the application of the SMD. From this point, we have removed the restrains and continued with free MD simulations for a total time of 120 ns. On the other hand, the BSA-2 molecule has spontaneously adsorbed onto the substrate by the B fragment [Fig. 3(d)], which contains the hydrophobic lipid-binding pocket.

To characterize the BSA position with respect to the substrate, we have determined the time evolution of the center of mass (CM) of the molecule and its two fragments (A and B) measured from the topmost graphene layer. Figure 3(e) (BSA-1) and Fig. 3(f) (BSA-2) show the Z coordinates of the three centers of mass (CMZ), the full molecule (CMBSA), the A fragment (CMA), and the B fragment (CMB). For the BSA-1/G0 system, the center of mass of the molecule moved upwards during the first 10 ns of the MD simulation, reflecting a weak repulsive interaction. When the SMD procedure was applied, the molecule gently made contact with the substrate. After the forced adsorption procedure ended, the B fragment remained adsorbed for the remaining simulation time with its center of mass located at a distance of nearly 2 nm from the topmost graphene layer of the substrate [Fig. 3(e)]. The A fragment was not adsorbed, showing a fluctuating behavior in the aqueous solution. For the BSA-2/G0 case, the center of mass of the molecule moved spontaneously towards the flat substrate during the first 10 ns of the MD simulation. Similarly to the BSA-1/G0 system, the B fragment was the molecular region adsorbed to the surface, with its center of mass positioned roughly at the same distance as in the BSA-1/G0 case, while the A fragment was not adsorbed and remained oscillating in the aqueous solution. After 120 ns, both configurations, BSA-1 [Figs. 3(g) and 3(i)] and BSA-2 [Figs. 3(h) and 3(j)], remained adsorbed onto the flat substrate by the B fragment.

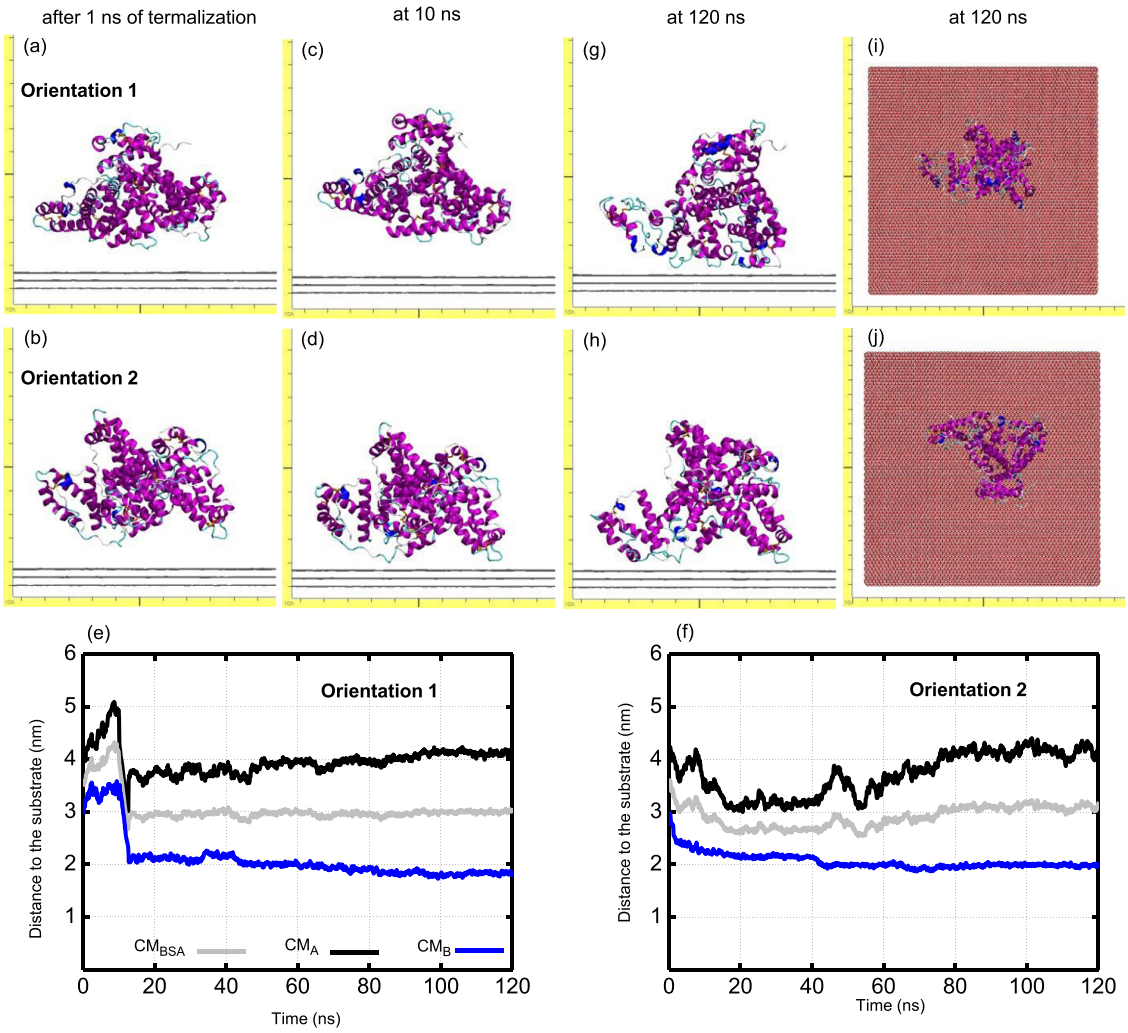

FIG. 3. Top row: snapshots of BSA-1 orientation over G0 substrate taken (a) after initial energy optimization and 1 ns of MD thermalization; (c) after 10 ns of the MD simulation; (g) and (f) after 120 ns of the MD simulation in side and top views, respectively. Second row: snapshots of BSA-2 orientation over G0 substrate taken (b) after initial energy optimization and 1 ns of MD thermalization; (d) after 10 ns of the MD simulation; (h) and (j) after 120 ns of the MD simulation in side and top views, respectively. Third row: (e) and (f) evolution of BSA-1 and BSA-2, respectively, Z coordinate of the center of mass corresponding to the full molecule (gray line), the A fragment (black line), and the B fragment (blue line).

B. BSA-1 and BSA-2 adsorption onto G3

The adsorption process of BSA-1 and BSA-2 has been also studied on the G3 stepped graphite substrate, with a step height slightly larger than 10 Å. Atomic structures after 1 ns of the thermalization process are shown in Figs. 4(a) and 4(b). At variance with the adsorption on the flat G0 substrate, BSA readily adsorbed to the stepped substrate in both orientations during the first 10 ns of the simulation [Figs. 4(c) and 4(d)]. Therefore, the behavior of the BSA-1/G3 system was strikingly different to the BSA-1/G0 system. Also differently, in the BSA-1/G3 system, both A and B fragments of the molecule were strongly adsorbed to the upper terrace of the step, as shown in the plots of the time evolution of the center of mass of the molecule and its two fragments [Fig. 4(e)] measured from the topmost graphene layer. During the following 120 ns of the MD simulation, the final positions of the three centers of mass (full molecule, A, and B fragments) evolved similarly until they reached values of approximately 2 nm. The final configuration for the BSA-1/G3 system [see Figs. 4(g) and 4(i)] confirmed that the BSA molecule was fully adsorbed.

In the BSA-2/G3 system, only the B fragment was adsorbed as in the BSA-2/G0 case. For both G3 and G0 substrates, the hydrophobic lipid-binding pocket of the fragment B approached the hydrophobic surface. However, the binding seems to be weaker in the BSA-2/G3 case, as shown by the final position of the center of mass of the fragment B, located at 2.7 nm from the topmost graphene layer [Fig. 4(f)]. The fragment A was not adsorbed and remained fluctuating in the aqueous solution [see Figs. 4(h) and 4(j)].

C. BSA-1 and BSA-2 adsorption onto G5

Finally, the adsorption processes of BSA-1 and BSA-2 have been studied on the G5 stepped graphite substrates with a step height close to 17 Å. Atomic structures after 1 ns of the thermalization process are shown in Figs. 5(a) and 5(b). As in the G3 substrate, in both orientations (BSA-1 and BSA-2), BSA is spontaneously adsorbed to the upper part of the step by the B fragment (containing the hydrophobic lipid-binding pocket) during the first 10 ns of MD [Figs. 5(c) and 5(d)]. In general, the BSA-2/G5 system behaves rather

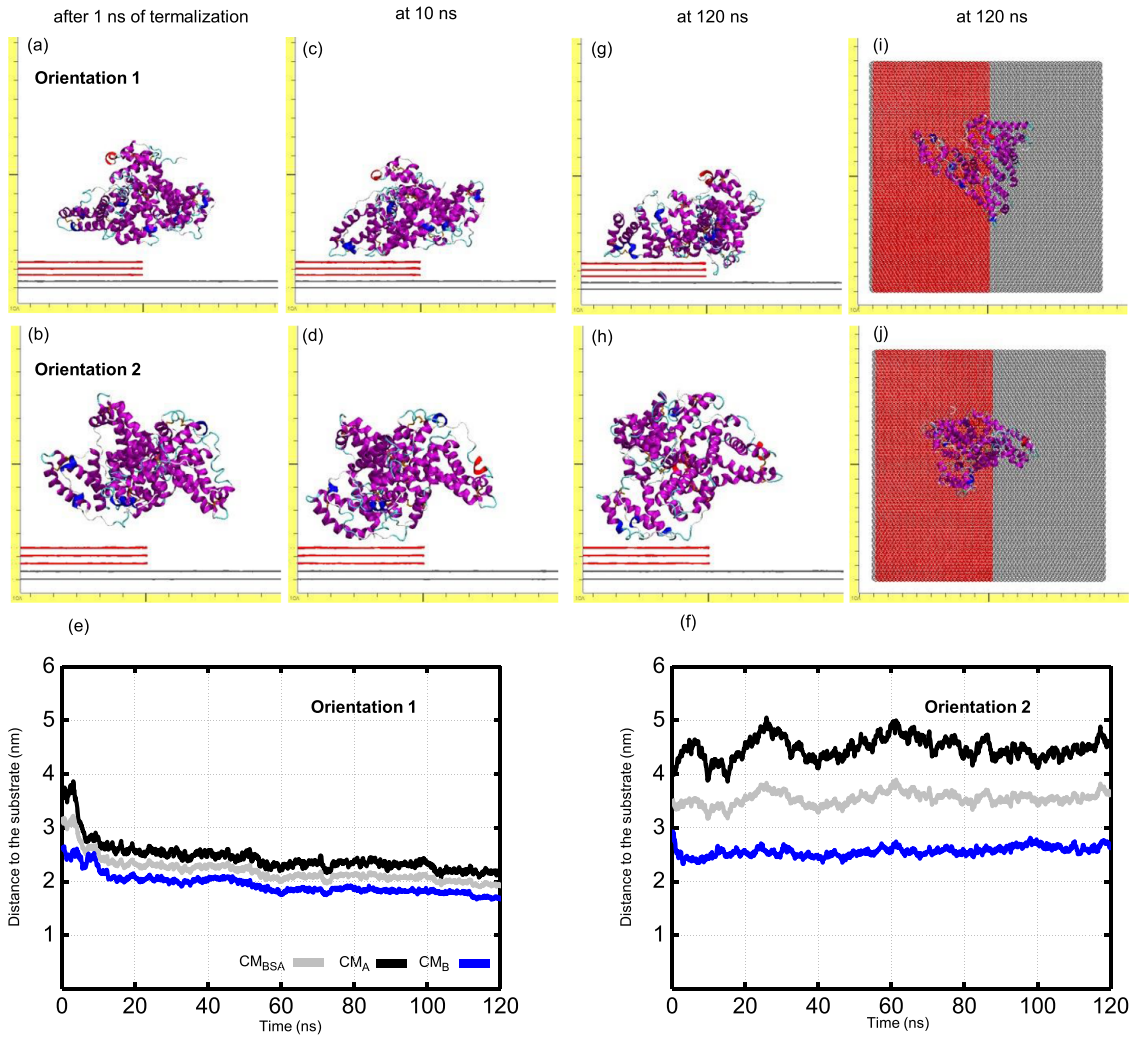

FIG. 4. Top row: snapshots of BSA-1 orientation over G3 substrate taken (a) after initial energy optimization and 1 ns of MD thermalization; (c) after 10 ns of the MD simulation; (g) and (f) after 120 ns of the MD simulation in side and top views, respectively. Second row: snapshots of BSA-2 orientation over G3 substrate taken (b) after initial energy optimization and 1 ns of MD thermalization; (d) after 10 ns of the MD simulation; (h) and (j) after 120 ns of the MD simulation in side and top views, respectively. Third row: (e) and (f) evolution of BSA-1 and BSA-2, respectively, Z coordinate of the center of mass corresponding to the full molecule (gray line), the A fragment (black line), and the B fragment (blue line).

similarly to the BSA-2/G3 system. However, in BSA-1/G5 case, the molecule/substrate interaction seems to be weaker than the BSA-1/G3 system, as only the B fragment is attached to the substrate. This attachment is clearly illustrated by the z coordinate of the center of mass of the molecule and its B fragment [Figs. 5(e) and 5(f)]. Subsequent MD evolution up to 120 ns [Figs. 5(g) and 5(j)] showed that the BSA molecule remained attached to the substrate by the B fragment whereas the A fragment oscillated in the aqueous solution. Interestingly, the top views in Figs. 5(i) and 5(j) reveal a relatively large displacement along the step-edge direction, this shift being especially evident in the BSA-2/G5 case. This point will be addressed in Sec. IV.

We also followed the evolution and stability of the BSA configuration for the six surface-protein systems under study by measuring (1) the root-mean-square-displacement (RMSD) and (2) the radius of the gyration tensor (RGT)-component parallel and perpendicular to the substrate of the α-carbon atoms of the protein. Figures S2–S4 of the supplementary material display plots of the RGT and the RMSD. RGT shows that, except for the BSA-1/G3 where both A and B fragments are adsorbed, the BSA molecule is enlarged in the direction perpendicular to the substrate due to the adsorption of just the B fragment and the up and down oscillatory motion of the non-adsorbed A fragment.

D. Contact surface areas and binding energies

Figures 6(a) and 6(b) show the time evolution of the contact surface area (CSA) for the six systems under consideration. The initial growth of the CSA for all the cases except BSA-1/G0 reflects that the adsorption process takes place spontaneously. In the BSA-1/G0 system, CSA starts to increase after the application of the SMD protocol. Final CSA values, with the exception of the BSA-1/G3 system, seem to be controlled by the protein adsorption orientation and are rather independent of the substrate morphology. CSA values for BSA-1 (in the 600–800 Å^2 range) are larger than those for BSA-2 (400–600 Å^2 range). The departure of the CSA for the BSA-1/G3 system from the general pattern is due

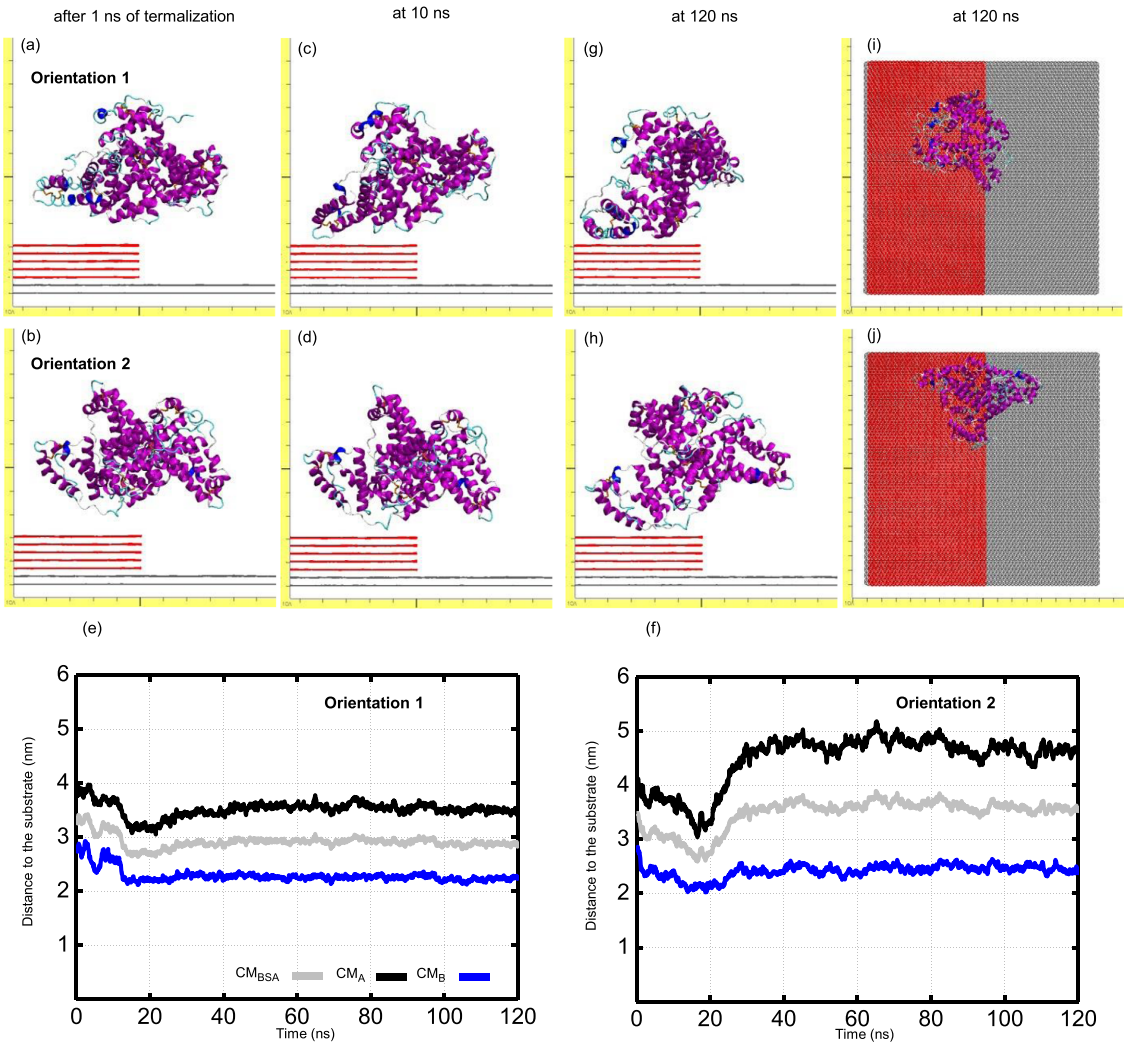

FIG. 5. Top row: snapshots of BSA-1 orientation over G5 substrate taken (a) after initial energy optimization and 1 ns of MD thermalization; (c) after 10 ns of the MD simulation; (g) and (f) after 120 ns of the MD simulation in side and top views, respectively. Second row: snapshots of BSA-2 orientation over G5 substrate taken (b) after initial energy optimization and 1 ns of MD thermalization; (d) after 10 ns of the MD simulation; (h) and (j) after 120 ns of the MD simulation in side and top views, respectively. Third row: (e) and (f) evolution of BSA-1 and BSA-2, respectively, Z coordinate of the center of mass corresponding to the full molecule (gray line), the A fragment (black line), and the B fragment (blue line).

to the fact that the BSA molecule slightly unfolds until the fragment A enters into contact with the lower part of the surface step.

In order to confirm whether the BSA-1/G3 and BSA-2/G3 configurations corresponded to equilibrium states, we have extended the MD simulations up to 200 ns for both systems. The final BSA-1/G3 and BSA-2/G3 configurations after 200 ns show no further structural modifications [compare Fig. 7 with Figs. 4(g) and 4(h) corresponding to 120 ns] and no further changes in CSA (Fig. S5 of the supplementary material). Therefore, the increasing CSA values observed in BSA-1/G3 at the end of 120 ns come from the adsorption of both fragments, A and B of the BSA molecule, onto the stepped substrate, which significantly enhanced the CSA compared with the processes observed for the G0 and G5 substrates.

Binding energies, calculated from Eq. (2), for the six molecule/substrate systems under study are plotted in Figs. 6(c) and 6(d). BSA-1 systems [Fig. 6(c)] present binding energy values in the range of 200–300 kcal/mol, higher than those found for BSA-2 systems [Fig. 6(d)] which are in the 100–200 kcal/mol range. A plot of the binding energy versus CSA values reveals a linear correlation between both quantities (Fig. S6 of the supplementary material), with slope values for all systems ranging from 26.7 to 33.6 kcal/mol nm^2 with a standard deviation of 2.4 kcal/mol nm^2. This correlation is consistent with the stronger binding energy found for the BSA-1/G3 system (300 kcal/mol) associated with the larger CSA [Fig. 6(a)].

E. Protein mobility

Information about the influence of the substrate morphology on the protein mobility can be gathered from the squared displacement (SD) of its center of mass (CM) during the simulations, $\Delta R^2(t, t_0) = \left(\bar{R}_{cm}(t) - \bar{R}_{cm}(t_0)\right)^2$, with $t_0 = 0$, the starting time of the MD run. Figure 8 shows the contribution to $\Delta R^2(t, t_0)$ from the three coordinate directions during the whole simulation, including the equilibration and forced/spontaneous adsorption stages, for the two adsorption orientations on the three different substrates. The CM

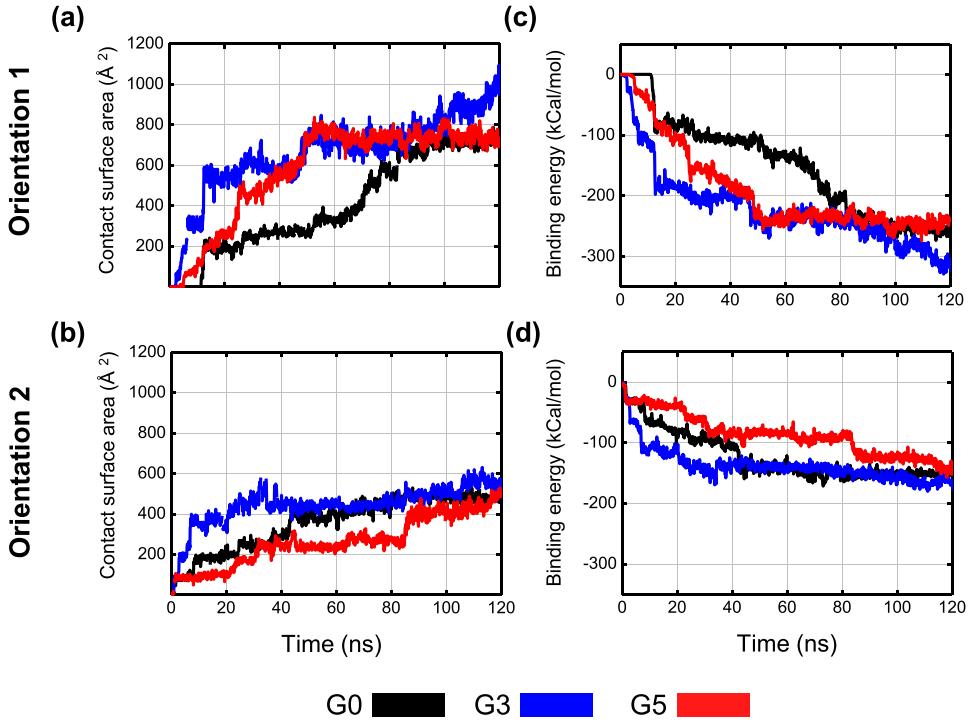

FIG. 6. Time evolution, during the 120 ns of the MD simulation, of the contact surface area (CSA) as calculated from Eq. (1) (left column) and binding energies as calculated from Eq. (2) (right column), for the two orientations of the BSA molecule: BSA-1, top row, and BSA-2, bottom row. The G0, G3, and G5 graphite substrates were considered.

trajectories for all systems are shown in Fig. S7 of the supplementary material. For the flat *G*0 substrate, the three contributions on the *x*, *y*, and *z* directions are small and seem to be independent of the protein orientation [Figs. 8(a) and 8(b)]. In the case of the G3 substrate, $\Delta R^2(t, t_0)$ values are only slightly increased [Figs. 8(c) and 8(d)].

The SD evolution dramatically changed for the BSA adsorption onto the G5 substrate where a clear increase in the SD was observed along the direction parallel to the step edge (*y* axis), as shown in Figs. 8(e) and 8(f). In the BSA-1/G5 system, the SD grows linearly during the first 40 ns of the MD run, when CSA values were below 600 Å^2, decreases during the next 10 ns, and oscillates in the 7-15 nm^2 range for $t > 50$ ns, where CSA stabilizes around 750 Å^2. The BSA-2/G5 system displayed a roughly linear increase in the value of the *y* contribution to $\Delta R^2(t, t_0)$ during the first 90 ns of MD,

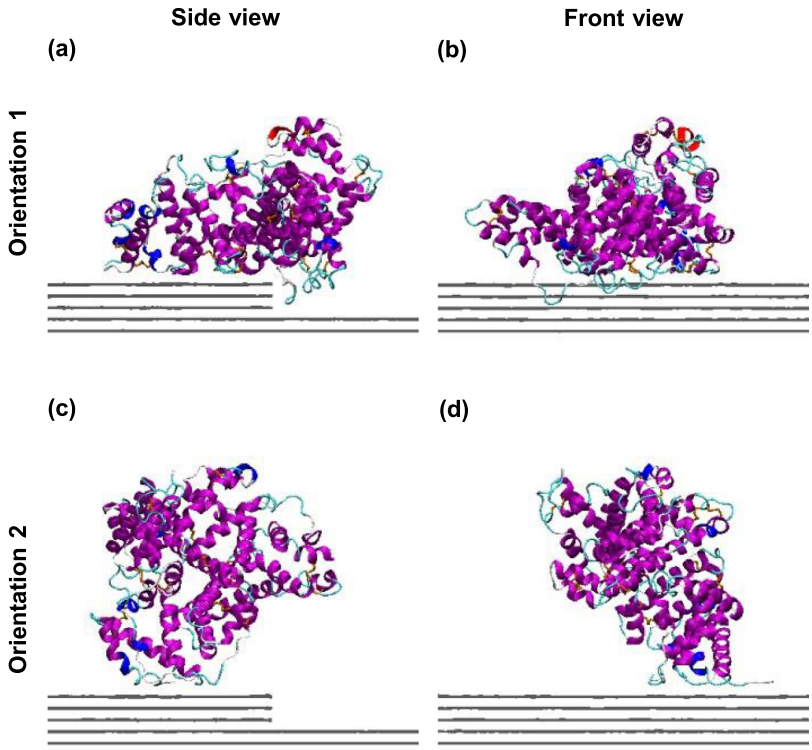

FIG. 7. (a) Side and (b) front views of the BSA-1/G3 system after 200 ns of the MD simulation. (c) and (d) for the BSA-2/G3 system.

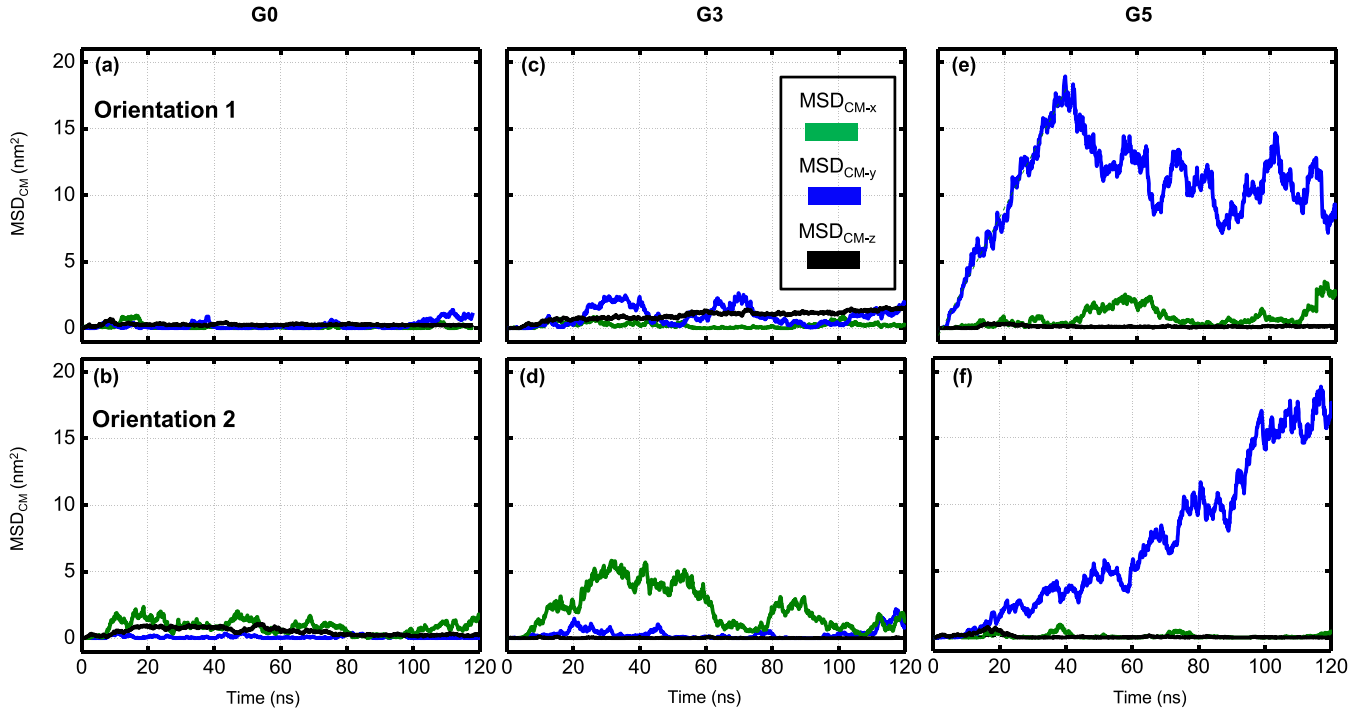

FIG. 8. Square Displacement (SD) of the X, Y, and Z coordinates of the Center of Mass (CM) for both BSA orientations, BSA-1 (top row) and BSA-2 (bottom row) onto the G0, G3, and G5 graphite substrates.

corresponding to CSA values below 400 Å^2, continued growing for later times, and seemed to stabilize in the last stages of the simulation. Thus, in all of the cases, we observed that a stable adsorption configuration (i.e., constant CSA) leads to a reduction or a stabilization of the SD. Nevertheless, the G5 surface stands out, as the fluctuations of the SD (i.e., back-and-forth movement along the step edge) are much higher than in the other substrates.

F. Protein conformation: Secondary structure and residue distribution at the contact area

The native BSA secondary structure is mainly composed of α-helix (73.8%), loops, bends and turns (13.2%), and some randomly oriented structures identified as random coils (13.0%). The secondary structure was analyzed using the set of atomic coordinates of BSA obtained at the end of the simulation for the six systems that we have studied. The results of this analysis are shown in Table I, where they are compared with those corresponding to the BSA structure obtained at the end of the thermalization stage. The important message is that a relatively small loss of α-helix content (from 7% to 15%) can be observed for all the cases. Table I shows that α-helix structures were transformed into other structures, such as a smaller diameter helix (3_{10} and π-helix), loops and turns, and random coils. Visual inspection shows that these changes in secondary structure are mostly located in the contact area, in agreement with other works.[12,20,29,32,45,72] The BSA-1/G0 system, where an SMD simulation was used to force adsorption, presented the largest loss of α-helix content (from 66.9% after the thermalization stage to 57.0% after 120 ns), but the difference is very small compared to the other substrates and orientations.

We also checked for significant rearrangements in the distribution of hydrophobic and hydrophilic amino-acid residues in the contact area due to the protein-substrate interaction. In particular, we examined the distribution of negatively (GLU and ASP) and positively (HIS, ARG, and LYS) charged amino-acid residues of the BSA molecule near the CSA. Figure 9 depicts the amino-acid residue distribution for the final configurations of the six systems, as seen from the graphite surface, in the volume defined by the topmost graphene layer and an horizontal plane located 1 nm above it. We did not find any marked preference of charged amino-acid residues to distribute over the graphite surface. This seems to be consistent with the fact that although the BSA molecule is negatively charged at the pH value of 7.4 considered in our simulations, the substrate is a neutral graphite slab whose carbon atoms have no partial charge. Furthermore, we confirmed the presence of both hydrophilic and hydrophobic amino-acids (displayed in gray in Fig. 9), as expected from the protein initial

TABLE I. Secondary structure percentage content after 120 ns of the MD simulation for both BSA orientations (BSA-1 and BSA-2) adsorbed onto three graphite substrates G0, G3, and G5.

System	α-helix	3_{10} and π-helix	Loops and turns	Random coils
BSA after therm.	66.9	2.92	17.84	12.35
BSA–1/G0	57.0	5.7	23.2	14.2
BSA–2/G0	62.3	4.0	20.9	12.9
BSA–1/G3	60.9	3.4	23.2	12.5
BSA–2/G3	59.7	5.8	21.4	13.0
BSA–1/G5	58.8	5.5	22.0	13.7
BSA–2/G5	61.1	3.8	22.5	12.7

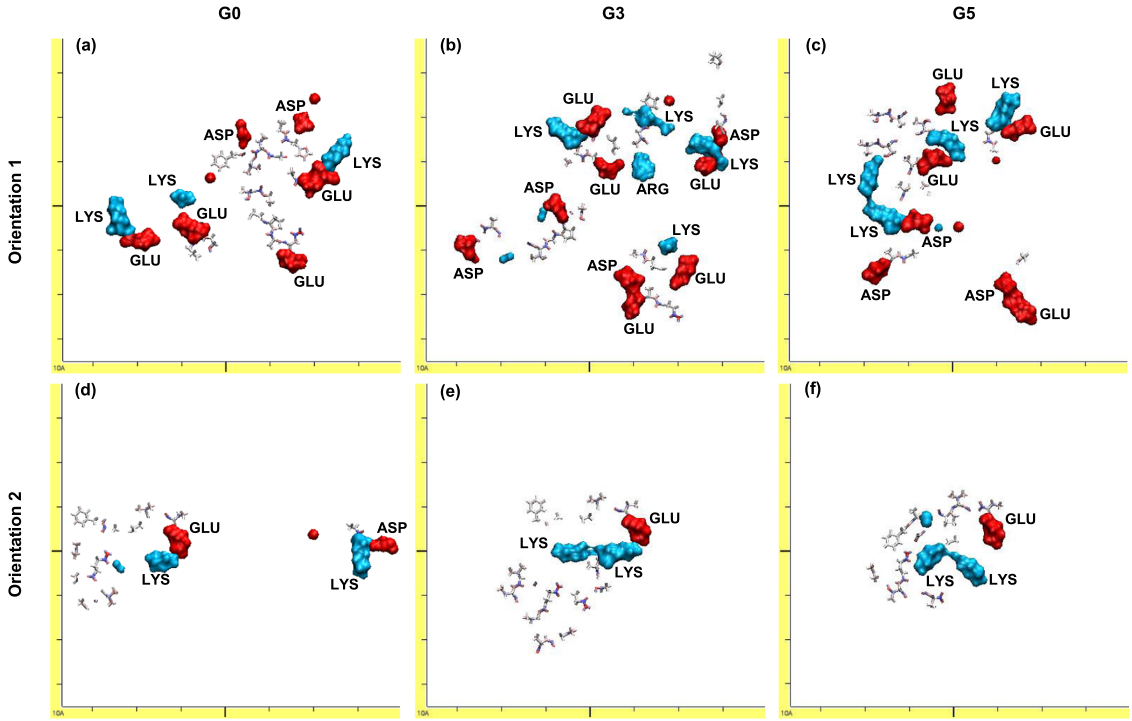

FIG. 9. Aminoacid distribution for the final protein adsorption configurations, as seen from the graphite surface, in the volume defined by the topmost graphene layer and an horizontal plane located 1 nm above it. The G0, G3, and G5 graphite substrates (columns) and the two BSA orientations (BSA-1, top row, BSA-2, bottom row) were considered. Negatively and positively charged residues are depicted in red and blue, respectively, while hydrophobic amino-acids are displayed in gray. Partial charges are assigned in accordance with the calculated ionization states of the titratable groups.

conformation, where active parts like the DSs present a combination of residues with different character.

IV. DISCUSSION

In Sec. III, we have presented the characterization of the adsorption process of BSA with two different orientations (BSA-1 and BSA-2) onto flat (G0) and stepped graphite substrates (G3 and G5). Based on these results as well as the ones presented in Ref. 45, we discuss now the influence of environmental conditions (such as the ion concentration) and the substrate morphology on the adsorption process.

A. Effect of the ionic concentration

Starting with the adsorption on the flat G0 substrate, we found that BSA-2 was readily adsorbed during the initial 10 ns of the simulation [see Fig. 3(f)]. On the contrary, BSA-1 did not spontaneously approach to the substrate, and a steered MD (SMD) simulation was necessary to bring the protein and substrate into contact [Fig. 3(e)]. This behavior differs from the one found in our previous simulations for this system,[45] where, instead of the physiological conditions used here by the inclusion of salt ions (Na^+, Cl^-) in a concentration of 140 mM plus the additional 12 Na^+ counter-ions for overall charge neutrality, we simulated pure water conditions (including only the Na^+ ions needed for charge neutrality). In that case, both orientations are spontaneously adsorbed on the substrate. This clearly shows the influence of the ion concentration on the adsorption on hydrophobic surfaces. Furthermore, not only the initial stages but also the final adsorption structures are affected by the ion concentration, as shown by the comparison of the corresponding CSA values: 7.6 (5.0) nm^2 for BSA-1 (BSA-2) under physiological conditions versus 9.2 (5.3) nm^2 for the free MD at 0 mM.

In a previous work,[45] we have shown that under neutralizing salt conditions (i.e., 0 mM), BSA DSs play a relevant role in the adsorption process. For BSA-1 orientation, the vicinity of these sites to the surface favors the initial adsorption to graphene and leads to a more strongly bound adsorption configuration. In Ref. 45, this behavior was explained via two different mechanisms: their hydrophobic nature and their flexibility. The former arises from the fact that DSs contain a large number of hydrophobic amino-acids[40] which promote the initial adsorption to a hydrophobic surface such as graphite if BSA orientation is favorable. As for the high flexibility of DSs,[40,45] they lead to a stronger final adsorption since they can better accommodate necessary deformations arising from the adsorption process. In contrast, for BSA-2 orientation, DSs are as farther away from the surface as possible as shown in Fig. 10. Therefore the effect of DSs on the adsorption along BSA-2 orientation (be it under physiological conditions considered here or with 0 mM of salt concentration considered in Ref. 45) is negligible, and BSA-2 adsorbs mainly in a non-specific manner to the substrate, i.e., mostly through van-der-Waals (vdW) forces.

Here, i.e., at physiological salt concentrations, we systematically observe (for G0, G3, and G5) that final adsorption energies and contact areas of BSA-1 are significantly larger than the ones obtained for BSA-2 (see Fig. 6). This difference indicates that the vicinity of DSs to the substrate stabilizes the final adsorption configuration both at 140 mM and 0 mM salt concentrations. In order to understand how DSs affect

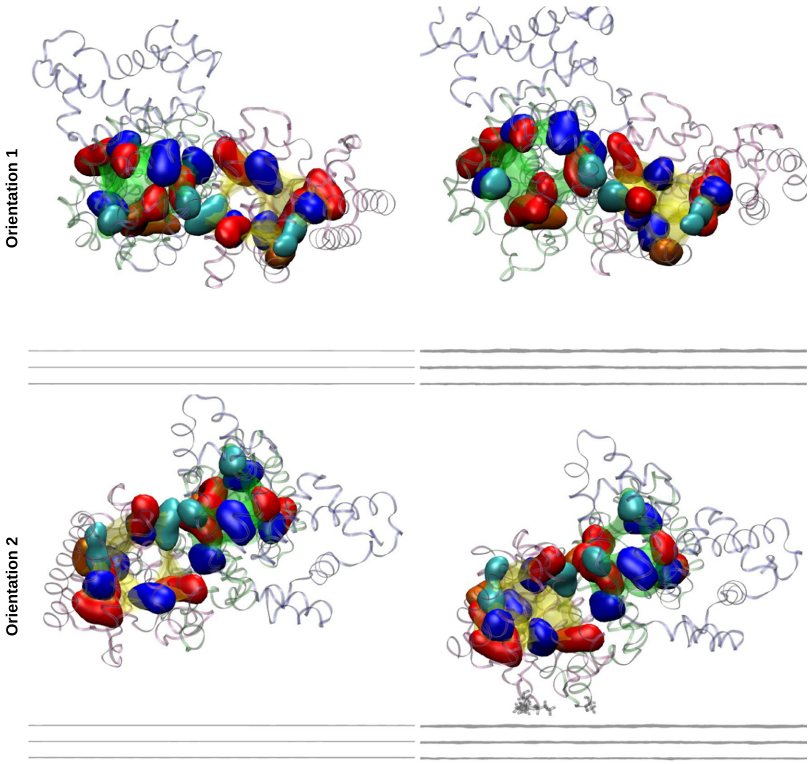

FIG. 10. Hydrophobic and hydrophilic amino-acid residue distribution for the Sudlow sites (DSs) on the BSA-1 (top row) and BSA-2 (bottom row) orientations. On the left column, we represent their structure under pure water conditions (0 mM), and on the right column, we represent their structure at physiological conditions (140 mM). The right column images correspond to the protein structure right before the application of the forced adsorption protocol. Hydrophobic/hydrophilic amino-acid residues are colored in accordance with their hydrophobicity index:[75] very hydrophilic, neutral, hydrophobic, and very hydrophobic residues are colored in red, orange, cyan, and dark blue, respectively. The DSs are highlighted by the green and yellow transparent surfaces. Under physiological conditions, the protein shields the strongly hydrophobic residue (in dark blue) at the bottom left while exposing the hydrophilic ones around it.

the initial stages of adsorption, we resort to their flexibility and hydrophobicity. In Fig. S8 of the supplementary material, we represent the DS2 structure at 0 mM and at 140 mM, while BSA is in solution. A careful inspection of Fig. S8 allows us to see that DSs adopt a more compact structure at 0 mM than at 140 mM. The opening of DSs at 140 mM is allowed by the random coils present in the pocket (acting as hinges) and promotes the outward movement of hydrophilic amino-acids. This can be better seen in Fig. 10, where, by looking at the bottom left part of each DS, it is clear that the protein shields the strongly hydrophobic residues (in dark blue) while exposing the hydrophilic ones around it. Therefore, at variance with the previous work,[45] where no salt was present in the solution, here the increased flexibility of the DSs is working against the initial adsorption to the surface. The flexibility of DSs is allowing hydrophilic amino-acids to move outward (see Fig. 10), thus creating an initial adsorption barrier. This barrier is felt by BSA-1 orientation by being unable to adsorb freely in our dynamics at 140 mM, contrary to all the other cases. For BSA-2, as these sites are pointing away from the surface (see Fig. 10), this rearrangement has little influence in the adsorption process. As a result, BSA-2 adsorbs spontaneously in a non-specific manner, i.e., mostly through van-der-Waals (vdW) interactions, as shown in Fig. 10.

Additionally, it is interesting to note that when comparing the contact areas of adsorption for the two cases, i.e., no salt (9.2/5.3 nm^2 BSA-1/BSA-2) and 140 mM of NaCl (7.6/5.0 nm^2 BSA-1/BSA-2), we observe that the orientation that is most affected by the ionic strength is BSA-1, which corroborates that this non-specific adsorption of BSA-2 is little affected by the presence of salt in solution. Note that although the same amino-acids rearrangement is occurring in stepped surfaces (G3 and G5), BSA-1 is able to freely adsorb to the substrate. In these cases, as shall be explained in detail in Subsection. IV B, the substrate morphology provides an alternate mechanism of adsorption (see Fig. S9 of the supplementary material).

Previous works[73,74] have shown that the ionic concentration [referred to as ionic strength (IS) in Ref. 73] has an important effect on the adsorption of proteins to charged surfaces. There the authors report the surface-protein interaction as a sum of vdW and electrostatic contributions. Therefore, by controlling the ionic strength of the solution, one could temper/enhance this interaction. Here our results indicate that the ionic-strength (IS) may also affect the adsorption of a hydrophilic protein (BSA, see Fig. S10 of the supplementary material) to a hydrophobic/uncharged substrate (graphite). Although surprising, as explained above, these results can be understood in terms of internal protein rearrangements occurring mostly in its flexible regions.

B. Effect of surface morphology and hydrophobicity

As shown in Figs. 3–5, the surface morphology results in a rich casuistry on the adsorption behavior of BSA. As we increase the number of layers, i.e., going from G0 to G5, the two key properties that might change are the protein substrate interaction and the morphology of the substrate. Below we discuss how these two affect the adsorption and which one is able to provide an explanation for the observed casuistry.

1. Substrate hydrophobicity

The wetting behavior, i.e., the hydrophobicity, of supported multi-layered graphene was a matter of great controversy[76,77] and only recently this has been solved for single

(1LG) and double layered graphene (2LG) surfaces.[78] In that work, Munz *et al.*[78] by using chemical force spectroscopy measurements demonstrated that the hydrophobicity of supported graphene depended on the number of deposited layers. In particular, in air conditions, they observed that 1LG, 2LG, and 3LG showed an increasing hydrophobicity, with the biggest difference observed between the 1LG and 2LG. Additionally, in conditions where the tip and the surface were fully embedded in water, they have again observed the same trend, i.e., 2LG was more hydrophobic (higher adhesion force) than 1LG. Nevertheless, due to the small amount of 3LG, they could not determine if the increasing hydrophobicity trend observed in air conditions for 3LG also applied in the full water embedding scenario.

In order to make a contact between our simulations and the force spectroscopy experiments in Ref. 78, one should consider the water affinity of BSA as a whole. BSA is a charged protein, whose surface amino-acids are mostly hydrophilic (see Fig. S10 of the supplementary material). In fact, BSA is a blood plasma protein (thus water soluble, i.e., hydrophilic) that works as a carrier of hydrophobic molecules in the blood stream (see Ref. 45 and references therein). Therefore, as a whole, BSA behaves as a hydrophilic protein, probing the interaction with the substrate in essentially the same way as the hydrophilic tip used in the force spectroscopy experiments in Ref. 78. Munz *et al.* (Fig. 2(b) in Ref. 78) observed a decrease in the adhesion of the hydrophilic tip with increasing surface hydrophobicity (1LG → 2LG → 3LG). Thus, in our case, an increase in the surface hydrophobic character should lead to a decrease in the BSA binding energy. When we compute the ratio between the binding energy and contact area (see Fig. S6 of the supplementary material), we observe that it decreases as we increase the number of graphene layers for both BSA orientations. Although one should take this observation with care, given the dispersion on the energy values, this trend is robust and seems to indicate that the increasing number of layers (G0 → G3 → G5) leads to an increasing hydrophobicity, in agreement with Munz *et al.*[78]

However, the trend described above is a minor effect (less than a 10% change in the binding energy/contact area ratio). This, together with its systematic character, cannot explain alone the rich behavior observed in our simulations. Assuming an increasing hydrophobicity from G0 to G5, we should expect a systematic decrease in the total binding energies. What we obtained (see Fig. 6) are very similar adsorption energies and contact areas for each of the orientations in all the different substrates. In all of the BSA-1 final adsorption configurations, the hydrophobic pockets are adsorbed to the substrate, what seems to be consistent with the total binding energies and the binding energy/contact area ratio being larger for this orientation. Thus, although the trend of increasing hydrophobicity is present, we cannot explain cases like BSA-1/G3, where the contact area and binding energy are larger than BSA-1/G5.

2. Substrate morphology

Below we carefully discuss how the surface morphology affects the adsorption of each protein fragment (A and B) in the two different orientations (BSA-2 and BSA-1).

In BSA-2, the Sudlow sites are far away from the substrate and play a negligible contribution to the adsorption of the protein as shown in Fig. 10. A close inspection of Figs. 3–5 indicates that the final distance to the substrate of the fragment A is 4.2, 4.6, and 4.7 nm for the G0, G3, and G5 substrates, respectively. Therefore, we can distinguish two different regimes: one where the non-adsorbed A-fragment is closer to the surface (G0) and another where it is farther away from it (G3 and G3). The substrate morphology seems to be the key to understand this difference. Note that, in G3 and G5, the A-fragment is the one that is hanging over the step. Figures. 3–5 show that BSA-2 systematically adsorbs non-specifically (i.e., by means of vdW forces) to the substrate via the B-fragment. This happens because of a very hydrophobic amino-acid located in a very flexible region near the substrate that promptly adsorbs to it (see Fig. S11 of the supplementary material). Once this region is anchored, the adsorption process proceeds through non-specific protein-substrate vdW interactions, first, by better adsorbing B-fragment and then the A-fragment follows (see Figs. 3–5). In the case of G3 and G5, the A-fragment has nowhere to anchor since it is at the edge of the step, and thus it remains fluctuating in the solution. In the G0 case, the A domain, after an initial transient where it seems to have adsorbed to the surface, detaches at t = 60 ns and remains so in the rest of the simulation. Nevertheless, its vicinity to the substrate in the G0 case, and the associated vdW interaction, makes it possible to stabilize its final adsorption orientation on a somewhat closer configuration to the surface as compared to G3 and G5 cases. Therefore, although hydrophobic forces do have a contribution, their role in the BSA-2 adsorption is not relevant and the results obtained for the BSA-2 A-fragment can be understood solely in terms of the surface morphology.

As for the BSA-2 fragment B, its final distance to the substrate is 2.0, 2.7, and 2.5 nm for the G0, G3, and G5 substrates, respectively. Again, we can distinguish two different regimes: one where the B-fragment is closer to the surface (G0) and another case where it is farther away from it (G3 and G5). We can link these differences to the substrate morphology through the analysis of Figs. 3(f), 4(f), and 5(f). They show that BSA-2 is clearly tilted in the stepped surfaces (G3 and G5) as compared to the flat G0 case. The extra "freedom" of the A-fragment in the G3 and G5 cases affects how the adsorption of the B-fragment takes place: by tilting the molecule, they induce a lift of the B-fragment as a whole [see Figs. 4(f) and 5(f)]. In G3 and G5, the initial lack of both non-specific vdW and hydrophobic interactions with the surface results in a freely oscillating A-fragment, and this is ultimately what also affects the adsorption of B-fragment. In the G0 case, we observe that, as in G3 and G5, the B-fragment is the one starting the adsorption process (see Fig. R5). Nevertheless, in this case, the vicinity of the A-fragment with the surface leads to its adsorption via non-specific vdW interactions as explained above. As a result, the final adsorption conformation on the G0 surface is flatter, i.e., not tilted, and therefore the center of mass of the B-fragment is closer to the substrate.

For BSA-1, the Sudlow sites are close to the surface (see Fig. 10), and, as before, both their flexibility as well as their

hydrophobic character play an important role in the adsorption process. From Figs. 3–5, we determine the final distances to the substrate of BSA-1 fragment A: 4.1, 2.1, and 3.5 nm for the G0, G3, and G5 substrates, respectively. This seems to indicate that the presence of steps allows the A-fragment to come closer to the substrate. First we focus on the difference between G0 and G3. While in the former, DSs adsorb in the same plane, in the latter, DS2 (shown in yellow) adsorbs on the top plane and DS1 (represented in green) adsorbs at the step edge. Having started the adsorption in the B fragment (see Fig. S9 of the supplementary material), the step edge is the only place left where DS1 hydrophobic pocket can adsorb. Note that this is also a place where the flexibility of DSs may be exploited to enhance the adsorption. Driven by this process, A-fragment adsorption followed with some of its amino-acids adsorbed also to the bottom layer thus stabilizes this adsorption configuration (see Fig. 4). Therefore, the difference in the final distance to the center of masses of the A-fragment between G0 and G3 can be attributed to the surface morphology. As for the G5 case, we think that the step height, and the resulting lack of vdW interactions between the A-fragment and the bottom surface, prevented a similar adsorption configuration as in G3 to happen, thus leaving the A floating in the solution.

As for the BSA-1 fragment B, we observe that, within a deviation of 10%, its center of mass is located at 2 nm from the substrate for all the cases (1.9, 1.8, and 2.2 nm for the G0, G3, and G5). The smaller value reported for G3 could be understood as a consequence of the adsorption of the A-fragment onto the bottom part of the substrate [see Fig. 4(g)] that took along with it the part of the B-fragment.

C. Protein mobility

The substrate morphology seems to offer the possibility to modify the protein mobility. While the G0 and G3 substrates rapidly anchored the BSA molecule [Figs. 8(a)–8(d)], graphite substrates with higher steps (G5) seem to enhance the protein diffusion in the direction parallel to the step edge in the early stages of the adsorption process [Figs. 8(e) and 8(f)]. The protein orientation modulates this effect, as reflected in the different behavior of BSA-1/G5 and BSA-2/G5 and also in the displacements observed in the direction perpendicular to the step for BSA-2 in the G0 and G3 substrates.

It is not easy to grasp the origin of this enhanced mobility. Protein diffusion can be enhanced by decreasing the protein concentration and increasing the salt concentration.[79] Experiments for BSA inside a nanostructured substrate like a 100 kDa Polyethersulfone (PES) membrane[80] have determined a diffusion coefficient of 3.8×10^{-7} cm^2/s at an ionic condition of 0.100M of KCl, pH of 6.8, and low protein concentration (0.5 g/dm^3). With all the precautions in the comparison, given the limited number of simulations that we have performed, our estimated diffusion coefficient in the direction parallel to the step edge reproduces the correct order of magnitude, being ∼3 times larger. This further enhancement could be attributed, following the experimental trend with concentration, to the limit of an isolated molecule considered in our simulations. Although the high mobility is not directly correlated with the binding energy or the CSA, the effect seems to disappear once the final, stable adsorption configuration is reached. Thus, it seems natural to link it with the reduced vdW interaction with the lower terrace, but the back and forth displacements in the direction perpendicular to the step for the G3 and G5 substrates (see Fig. S7 of the supplementary material) point out to a more complex scenario. We speculate that the water configuration around the step may play a role. More simulations are necessary to firmly substantiate this enhanced mobility and to understand its origin, but our results suggest that stepped surfaces may favor well-ordered protein adsorbed structures.

D. Protein conformation: Secondary structure and residue distribution at the contact area

Changes in protein conformation upon adsorption are critical to biosensing applications, as these conformational changes may cause structural hindrances that impair the recognition efficiency of hydrophobic ligands.[81] Our results clearly show a very modest change in the secondary structure, irrespective of the orientation and the substrate morphology, in agreement with both our previous works for a flat surface under pure water conditions[45] and with recent experimental findings.[11] The losses in α–helical content are around 10%–15% (7%-10%) for BSA-1 (BSA-2) orientations. These changes are mostly confined to the contact area. There is no contradiction between these results and the common consideration of BSA as a soft protein. Forced adsorption simulations of BSA on this same substrate (Ref. 45) show that, by applying an external force, one is able to significantly deform BSA. However, the changes induced in BSA as a result of the free adsorption were much less severe than the ones introduced by the application of the force. Furthermore, once the external force was removed, we observed[45] a gradual slow increase in the alpha-helical content of the protein. Therefore, our simulations indicate that although BSA is a soft protein, i.e., it easily deforms by the action of an external load, its structure seems to be quite resilient in a free adsorption process. For the systems where the fragment A was not adsorbed, the exposed domains preserved their structure and thus their functionality upon adsorption. These findings support the possible biofunctionalization of graphene layers with albumin, in agreement with what has been observed experimentally and theoretically for the immunoglobulin-G.[20]

Finally, we address the contribution of different interactions to the protein adsorption. The observed non-preferential distribution of charged amino-acid residues of the BSA molecule in the contact area and the linear relation between binding energy and CSA indicate that vdW interactions play a dominant role. A recent MD study for the adsorption of bovine fibrinogen (BFG) on graphene has reached the same conclusion.[82] However, the differences in binding energy between the two orientations found in our simulations point towards a non-negligible contribution of hydrophobic forces. Orientations that expose DS or fatty-acid binding sites to the substrate are more strongly bonded. The absence of a massive rearrangement of hydrophobic and hydrophilic residues observed in our simulations may seem to rule out this contribution but the effect is more subtle. These binding sites have a complex structure, biologically designed to bind certain specific

molecules, and are located at very flexible zones of the protein, so they can open and close easily. They usually expose a hydrophilic residue that captures the hydrophilic part of the fatty acids, while, at the core, they have a bunch of very hydrophobic amino-acids. These complex structures explain why we found a mix of hydrophobic/hydrophilic amino-acids in the contact. The flexibility is a key ingredient to understand our apparently contradicting results. This flexibility is responsible for the structural changes of the DSs under physiological conditions, hiding (exposing) the hydrophobic(phylic) residues, that prevent spontaneous adsorption for the BSA-1/G0 system. On the other hand, it is this same flexibility that allows those amino-acids to spread out, once the contact is forced and water excluded, in order to increase the contact area with a hydrophobic substrate like graphene. This larger contact area increases the vdW interaction, explaining the larger adsorption energies for BSA-1 orientation, and contributes to the binding with hydrophobic interactions that results in different coefficients (between BSA-1 and BSA-2) for the linear relation between the adsorption energy and contact area.

V. CONCLUSIONS

We have studied the influence of the substrate morphology on the adsorption of bovine serum albumin (BSA) with long MD simulations (up to 200 ns) using the AMBER[56] suite and an explicit solvation method (TIP3P). In particular, to account for different surface morphologies we have considered three different substrates, i.e., flat graphite (G0) and two stepped graphite surfaces (G3 and G5) with different step heights. In all these substrates we studied the role played by the surface morphology on the BSA adsorption along two orientations where the DS binding sites are exposed (BSA-1) or not (BSA-2) to the substrate. The comparison of our MD simulations under physiological conditions with our previous work,[45] performed under pure water conditions, allows us to address the influence of the ionic concentration in the adsorption process. The evolution of the system and the final adsorption configuration have been characterized through the analysis of the binding energies, contact surface areas (CSA), the RMSD of the center of mass of the molecule, and the individual fragments along the MD trajectories. Additional information comes from the changes in the secondary structure and the distribution of hydrophobic and hydrophilic residues in the protein-substrate contact area.

Our results show that both the ion concentration and the substrate morphology play a crucial role in the adsorption process. Stepped substrates favor the spontaneous adsorption of the protein, while also seem to lead to an enhanced protein mobility, particularly for the BSA-2 orientation. The adsorption of the BSA-1 orientation on flat surfaces under physiological conditions had to be gently forced through a steered MD protocol, at variance with the results for pure water, where both orientations are readily adsorbed. Our analysis confirm a very modest change in the protein secondary structure irrespective of the orientation and the substrate morphology, in agreement with our previous results for a flat surface under pure water conditions, with a small loss in the α–helical content around 10%–15% (7%–10%) for BSA-1 (BSA-2) orientations. These changes are essentially confined to the contact area, supporting the possible biofunctionalization of graphene layers with albumin. Binding energies are proportional to the contact area pointing towards a dominant role of vdW interactions. However, the protein orientation exposing the hydrophobic lipid-binding pocket to the substrate shows systematic adsorption structures with larger contact areas, stronger binding energies, and larger coefficients in the linear relation between the contact area and adsorption energy. These binding sites have a complex structure that includes both hydrophilic and hydrophobic amino-acids and are located at very flexible zones of the protein. This flexibility resolves the apparent contradiction between these results and the behaviour of the BSA-1 orientation in the first stages of the adsorption on flat surfaces. Flexibility allows the structural changes of the DSs under physiological conditions, hiding (exposing) the hydrophobic(phylic) residues, that prevent spontaneous adsorption for the BSA-1/G0 system. On the other hand, it is this same flexibility that allows amino-acids to spread out, once the contact is forced and water excluded, increasing the contact area (and thus the vdW interaction) with a hydrophobic substrate like graphene and contributing to the binding with hydrophobic interactions that result in different coefficients for the linear relation between the adsorption energy and contact area.

Due to the similarity between human serum albumin (HSA) and the BSA, we expect the results obtained here to apply also to the HSA molecule. We hope that our conclusions regarding the role of the ion concentration and surface morphology will stirr more theoretical and experimental work on the protein adsorption onto graphite stepped surfaces and contribute with helpful insights to the design of biomolecular sensors.

SUPPLEMENTARY MATERIAL

See supplementary material for the complete albumin (BSA) adsorption study onto graphite stepped surfaces, snapshots of the configuration of the BSA-1 adsorption on the G0 substrate, the time evolution of the contact surface area (CSA) for BSA-1 on the G3 substrate; and for all the systems studied, the time evolution of the parallel and perpendicular components of the radius of gyration tensor (RGT) and the root-mean-square-distance (RMSD) of BSA, correlation analysis between the binding energies and the contact surface area (CSA) between BSA and the substrates, and finally, trajectories of the center of mass (CM) of BSA.

ACKNOWLEDGMENTS

We acknowledge the financial support from the Spanish MINECO (Project Nos Consolider Force-For-Future CSD2010-00024, MAT2011-023627, MAT2012-2448, FIS2015-69295-C3-1-P, MAT2013-44858-R, and MAT2014-54484-P) and Comunidad de Madrid (No. S2009/MAT-1467), and also the computer resources, technical expertise, and assistance provided by the Red Española de Supercomputación at the Minotauro Supercomputer (BSC, Barcelona) and the Extremadura Research Centre for Advanced Technologies

(CETA-CIEMAT). P. Rubio-Pereda acknowledges support from CONACyT under scholarship No. 242867.

[1] R. K. Roy and K. L. Lee, J. Biomed. Mater. Res., Part B **83B**, 72 (2007).
[2] A. Grill, Diamond Relat. Mater. **12**, 166 (2003).
[3] H. Liu and T. J. Webster, Biomaterials **28**, 354 (2007).
[4] R. Aoki, T. Arakawa, N. Misawa, R. Tero, T. Urisu, A. Takeuchi, and T. Ogino, Surf. Sci. **601**, 4915 (2007).
[5] P. Roach, D. Farrar, and C. C. Perry, J. Am. Chem. Soc. **127**, 8168 (2005).
[6] M. Rabe, D. Verdes, and S. Seeger, Adv. Colloid Interface Sci. **162**, 87 (2011).
[7] S. Handschuh-Wang, T. Wang, S. I. Druzhinin, D. Wesner, X. Jiang, and H. Schnherr, Langmuir **33**, 802 (2017).
[8] H.-Y. Chen, D. Han, Y. Tian, R. Shao, and S. Wei, Chem. Phys. **430**, 13 (2014).
[9] M. Hofmann, Y.-P. Hsieh, A. L. Hsu, and J. Kong, Nanoscale **6**, 289 (2014).
[10] D. A. Puleo and R. Bizios, *Biological Interactions on Materials Surfaces* (Springer-Verlag, New York, 2009).
[11] A. P. A. Raju, S. C. Offerman, P. Gorgojo, C. Valles, E. V. Bichenkova, H. S. Aojula, A. Vijayraghavan, R. J. Young, K. S. Novoselov, I. A. Kinloch, and D. J. Clarke, RSC Adv. **6**, 69551 (2016).
[12] J. I. Paredes and S. Villar-Rodil, Nanoscale **8**, 15389 (2016).
[13] A. Alshammari, M. G. Posner, A. Upadhyay, F. Marken, S. Bagby, and A. Ilie, ACS Appl. Mater. Interfaces **8**, 21077 (2016).
[14] G. Y. Chen, D. W.-P. Pang, S.-M. Hwang, H.-Y. Tuan, and Y.-C. Hu, Biomaterials **33**, 418 (2012).
[15] Z. M. Markovic, L. M. Harhaji-Trajkovic, B. M. Todorovic-Markovic, D. P. Kepic, K. M. Arsikin, S. P. Jovanovic, A. C. Pantovic, M. D. Dramicanin, and V. S. Trajkovic, Biomaterials **32**, 1121 (2011).
[16] C. Heo, J. Yoo, S. Lee, A. Jo, S. Jung, H. Yoo, Y. H. Lee, and M. Suh, Biomaterials **32**, 19 (2011).
[17] Y. Cai, H. Li, B. Du, M. Yang, Y. Li, D. Wu, Y. Zhao, Y. Dai, and Q. Wei, Biomaterials **32**, 2117 (2011).
[18] L. Feng, Y. Chen, J. Ren, and X. Qu, Biomaterials **32**, 2930 (2011).
[19] G. Zhang, *Computational Bioengineering* (CRC Press, 2015), pp. 293–326.
[20] J. G. Vilhena, A. C. Dumitru, E. T. Herruzo, J. I. Mendieta-Moreno, R. Garcia, P. A. Serena, and R. Perez, Nanoscale **8**, 13463 (2016).
[21] G. López-Polín, M. Ortega, J. Vilhena, I. Alda, J. Gomez-Herrero, P. A. Serena, C. Gomez-Navarro, and R. Pérez, Carbon **116**, 670 (2017).
[22] G. Raffaini and F. Ganazzoli, Macromol. Biosci. **7**, 552 (2007).
[23] G. Raffaini and F. Ganazzoli, Langmuir **29**, 4883 (2013).
[24] G. Raffaini and F. Ganazzoli, Langmuir **26**, 5679 (2010).
[25] F. Ganazzoli and G. Raffaini, Phys. Chem. Chem. Phys. **7**, 3651 (2005).
[26] G. Raffaini and F. Ganazzoli, Langmuir **19**, 3403 (2003).
[27] C. Mücksch and H. M. Urbassek, Chem. Phys. Lett. **510**, 252 (2011).
[28] C. Mücksch and H. M. Urbassek, PLoS One **8**, e64883 (2013).
[29] D. Horinek, A. Serr, M. Geisler, T. Pirzer, U. Slotta, S. Q. Lud, J. A. Garrido, T. Scheibel, T. Hugel, and R. R. Netz, Proc. Natl. Acad. Sci. U. S. A. **105**, 2842 (2008).
[30] T. Wei, M. A. Carignano, and I. Szleifer, Langmuir **27**, 12074 (2011).
[31] L. Ou, Y. Luo, and G. Wei, J. Phys. Chem. B **115**, 9813 (2011).
[32] T. Wei, M. A. Carignano, and I. Szleifer, J. Phys. Chem. B **116**, 10189 (2012).
[33] Y. Allieu, M. Winter, J. P. Pequignot, and P. de Mourgues, Eur. J. Orthop. Surg. Traumatol. **16**, 1 (2006).
[34] L. Zhen, H. Mengyuan, X. Dangdang, and L. Zhihong, J. Photochem. Photobiol., C **18**, 1 (2014).
[35] Y. Zhang, T. R. Nayak, H. Hong, and W. Cai, Nanoscale **4**, 3833 (2012).
[36] F. De Leo, A. Magistrato, and D. Bonifazi, Chem. Soc. Rev. **44**, 6916 (2015).
[37] S. F. Oliveira, G. Bisker, N. A. Bakh, S. L. Gibbs, M. P. Landry, and M. S. Strano, Carbon **95**, 767 (2015).
[38] H. Shen, L. Zhang, M. Liu, and Z. Zhang, Theranostics **2**, 283 (2012).
[39] D. Carter and J. X. Ho, *Advances in Protein Chemistry* (Academic Press, New York, 1994), Vol. 45, pp. 153–203.
[40] A. Bujacz, Acta Crystallogr., Sect. D: Biol. Crystallogr. **68**, 1278 (2012).
[41] E. L. Gelamo, C. H. T. P. Silva, H. Imasato, and M. Tabak, Biochim. Biophys. Acta, Protein Struct. Mol. Enzymol. **1594**, 84 (2002).
[42] C. F. Wertz and M. M. Santore, Langmuir **17**, 3006 (2001).
[43] B. Langdon, M. Kastantin, and D. Schwartz, Biophys. J. **102**, 2625 (2012).
[44] B. Sivaraman and R. A. Latour, Langmuir **28**, 2745 (2012).
[45] J. G. Vilhena, P. Rubio-Pereda, P. Vellosillo, P. A. Serena, and R. Pérez, Langmuir **32**, 1742 (2016).
[46] J. Wang, R. M. Wolf, J. W. Caldwell, P. A. Kollman, and D. A. Case, J. Comput. Chem. **25**, 1157 (2004).
[47] J. P. Brandt, T. W. Patapoff, and S. R. Aragon, Biophys. J. **99**, 905 (2010).
[48] J.-L. Tsai and J.-F. Tu, Mater. Des. **31**, 194 (2010).
[49] J. G. Vilhena, C. Pimentel, P. Pedraz, F. Luo, P. A. Serena, C. M. Pina, E. Gnecco, and R. Pérez, ACS Nano **10**, 4288 (2016).
[50] G. Das, F. Mecarini, F. Gentile, F. D. Angelis, H. M. Kumar, P. Candeloro, C. Liberale, G. Cuda, and E. D. Fabrizio, Biosens. Bioelectron. **24**, 1693 (2009).
[51] M. Arnold, M. Schwieder, J. Blummel, E. A. Cavalcanti-Adam, M. Lopez-Garcia, H. Kessler, B. Geiger, and J. P. Spatz, Soft Matter **5**, 72 (2009).
[52] H. M. Berman, J. Westbrook, Z. Feng, G. Gilliland, T. N. Bhat, H. Weissig, I. N. Shindyalov, and P. E. Bourne, Nucleic Acids Res. **28**, 235 (2000).
[53] J. C. Gordon, J. B. Myers, T. Folta, V. Shoja, L. S. Heath, and A. Onufriev, Nucleic Acids Res. **33**, W368 (2005).
[54] R. Rhoades and D. Bell, *Medical Physiology: Principles for Clinical Medicine* (Lippincott Williams & Wilkins, 2012).
[55] A. Shkilnyy, P. Proulx, J. Sharp, M. Lepage, and P. Vermette, Colloids Surf., B **93**, 202 (2012).
[56] D. A. Case, T. A. Darden, T. E. Cheatham III, C. L. Simmerling, J. Wang, R. E. Duke, R. Luo, R. C. Walker, W. Zhang, K. M. Merz, B. Roberts, S. Hayik, A. Roitberg, G. Seabra, J. Swails, A. W. Götz, I. Kolossváry, K. F. Wong, F. Paesani, J. Vanicek, R. M. Wolf, J. Liu, X. Wu, S. R. Brozell, T. Steinbrecher, H. Gohlke, Q. Cai, X. Ye, J. Wang, M.-J. Hsieh, G. Cui, D. R. Roe, D. H. Mathews, M. G. Seetin, R. Salomon-Ferrer, C. Sagui, V. Babin, T. Luchko, S. Gusarov, A. Kovalenko, and P. A. Kollman, AMBER 12, University of California, San Francisco, 2012.
[57] R. Salomon-Ferrer, A. W. Gtz, D. Poole, S. Le Grand, and R. C. Walker, J. Chem. Theory Comput. **9**, 3878 (2013).
[58] T. P. King, Arch. Biochem. Biophys. **156**, 509 (1973).
[59] P. Jost and O. Griffith, *Lipid-Protein Interactions*, Lipid-protein Interactions No. V. 1 (Wiley, 1982).
[60] C. Mücksch and H. M. Urbassek, Langmuir **27**, 12938 (2011).
[61] Y. Xie, J. Zhou, and S. Jiang, J. Chem. Phys. **132**, 065101 (2010).
[62] M. Deighan and J. Pfaendtner, Langmuir **29**, 7999 (2013).
[63] C. Peng, J. Liu, D. Zhao, and J. Zhou, Langmuir **30**, 11401 (2014).
[64] J. Liu, C. Liao, and J. Zhou, Langmuir **29**, 11366 (2013).
[65] W. L. Jorgensen, J. Chandrasekhar, J. D. Madura, R. W. Impey, and M. L. Klein, J. Chem. Phys. **79**, 926 (1983).
[66] A. W. Götz, M. J. Williamson, D. Xu, D. Poole, S. Le Grand, and R. C. Walker, J. Chem. Theory Comput. **8**, 1542 (2012).
[67] D. R. Roe and T. E. Cheatham, J. Chem. Theory Comput. **9**, 3084 (2013).
[68] M. L. Connolly, J. Appl. Crystallogr. **16**, 548 (1983).
[69] W. Kabsch and C. Sander, Biopolymers **22**, 2577 (1983).
[70] R. P. Joosten, T. A. H. te Beek, E. Krieger, M. L. Hekkelman, R. W. W. Hooft, R. Schneider, C. Sander, and G. Vriend, Nucleic Acids Res. **39**, D411 (2010).
[71] A. R. Leach, *Molecular Modelling: Principles and Applications* (Prentice Hall, Harlow, New York, 2001).
[72] C. Ge, J. Du, L. Zhao, L. Wang, Y. Liu, D. Li, Y. Yang, R. Zhou, Y. Zhao, Z. Chai, and C. Chen, Proc. Natl. Acad. Sci. U. S. A. **108**, 16968 (2011).
[73] J. Liu, C. Peng, G. Yu, and J. Zhou, Langmuir **31**, 10751 (2015).
[74] C. Peng, J. Liu, Y. Xie, and J. Zhou, Phys. Chem. Chem. Phys. **18**, 9979 (2016).
[75] O. D. Monera, T. J. Sereda, N. E. Zhou, C. M. Kay, and R. S. Hodges, J. Pept. Sci. **1**, 319 (1995).
[76] J. Rafiee, X. Mi, H. Gullapalli, A. V. Thomas, F. Yavari, Y. Shi, P. M. Ajayan, and N. A. Koratkar, Nat. Mater. **11**, 217 (2012).
[77] Nat. Mater. **12**, 865 (2013).
[78] M. Munz, C. E. Giusca, R. L. Myers-Ward, D. K. Gaskill, and O. Kazakova, ACS Nano **9**, 8401 (2015).
[79] F. Roosen-Runge, M. Hennig, T. Seydel, F. Zhang, M. W. Skoda, S. Zorn, R. M. Jacobs, M. Maccarini, P. Fouquet, and F. Schreiber, Biochim. Biophys. Acta, Proteins Proteomics **1804**, 68 (2010).
[80] S. Salgn, S. Taka, and T. H. Zdamar, J. Mem. Sci. **278**, 251 (2006).
[81] F. Moreno, M. Cortijo, and J. González-Jiménez, Photochem. Photobiol. **69**, 8 (1999).
[82] Z. Gu, Z. Yang, L. Wang, H. Zhou, C. A. Jimenez-Cruz, and R. Zhou, Sci. Rep. **5**, 10873 (2015).